Robust design of vibro-impacting geared systems with uncertain tooth profile modifications via bifurcation tracking

Adrien Mélot, Emmanuel Rigaud, Joël Perret-Liaudet

Robust design of vibro-impacting geared systems with uncertain tooth profile modifications via bifurcation tracking

Adrien Mélot[a,*], Emmanuel Rigaud[a] and Joël Perret-Liaudet[a]

[a]*Laboratoire de Tribologie et Dynamique des Systèmes, UMR CNRS 5513, Ecole Centrale de Lyon, 36 avenue Guy de Collongue, 69134 Ecully Cedex, France*

ARTICLE INFO

Keywords:
Tooth profile modifications
Harmonic balance method
Nonlinear gear dynamics
Numerical continuation
Manufacturing errors
Vibro-impacts

ABSTRACT

The present work investigates the influence of uncertain tooth profile modifications on the nonlinear dynamic response of a spur gear pair induced by a backlash nonlinearity. To this end, an original approach based on bifurcation tracking is developed. The equations of motion are solved in the frequency domain with the harmonic balance method (HBM) coupled to an arc-length continuation algorithm and a bordering technique. The evolution of the bifurcation points with respect to the uncertain parameter is computed in a deterministic way. The study focuses on minimizing the amplitude-jump instabilities induced by the backlash nonlinearity around the primary resonance peak. The proposed methodology allows for a fast and reliable estimation of the tooth profile modification that minimizes the amplitude-jump instability by defining two criteria using the results of the bifurcation tracking algorithm. Probability density functions (PDF) of various indicators of the severity of vibro-impacts can be computed with Monte-Carlo (MC) simulation with minimal computational burden. Results show that the tooth profile modification that minimizes the amplitude-jump instabilities differs from the optimum obtained with static computations.

1. Introduction

Vibration and noise mitigation in geared system remains to this day a major challenge and research interest. The reasons are twofold. Firstly, large vibration amplitudes induce wear, fatigue and can compromise the structural integrity of the system. Secondly, vibrations generated at the gear are transferred to the housing via the shafts and bearings, which creates an unwanted noise: whining noise in case of permanent contact [6], or hammering or rattle noise when the response exhibits vibro-impacts [32, 34].

The meshing process is the origin of the transmission error and mesh stiffness fluctuations, which are assumed to be the main sources of excitation in geared systems. The former is defined as the difference between the actual position of the ouput gear and the position it would occupy, were the gear pair perfectly conjugate [40]; the latter is expressed as the derivative of the transmitted load with respect to the transmission error. Modifications of the gear micro-geometry, i.e. the profile of the tooth flanks, are commonly employed to optimize contact conditions, compensate for manufacturing defects and minimize the gear dynamic response. Such modifications consist in an intentional removal of material from the tooth flanks so that the tooth profile differs from the theoretical perfect involute. Their effect on both the static and dynamic responses of geared systems are well known [14, 20, 30, 19]. Most studies aim at minimizing the fluctuations of the transmission error to mitigate the dynamic response. This is traditionally carried out by optimizing the tooth profile modifications through static computations [36, 3, 5, 12]. Very few studies carry out dynamic analyses to define the best TPM, which often lead to different optimal solutions [24, 10, 30]. Such works try to minimize the peak-to-peak (DTE_{PP}) or the the root mean square values (DTE_{RMS}) of the dynamic transmission error. However such studies rely on computations of the dynamic response over the full range of operating rotational speed for a few discrete values of tooth profile modifications which can result in a significant computational effort.

Uncertainties in the system parameters are unavoidable due to manufacturing tolerances, wear, etc. They are seldom taken into account in dynamics analyses, all the more when the backlash nonlinearity is considered, since the associated computational costs are prohibitive. Tobe investigated the effect of random tooth-to-tooth errors on the dynamic behaviour of a gear pair both numerically [37] with Monte-Carlo simulations and experimentally [38]. Driot investigated the variability of the gearbox whining noise [9] and modal characteristics [8] induced by gear manufacturing tolerances. Uncertainties in the torque fluctuations were studied [2] with polynomial chaos expansion. Guerine [17] employed perturbation techniques to investigate uncertain structural parameters. Wei [39] implemented the incremental harmonic balance solver with the Chebyshev inclusion function to study the effects on uncertainties in the mesh stiffness, static transmission error, damping ratio and torque fluctuations.

Bifurcation tracking is a method to carry out parametric analyses of nonlinear systems. The first attempts at numerically tracking bifurcations date back to the 1970s. This type of dynamic analysis has gained a lot of attention in recents years, following the papers from Detroux [7] and Xie [41]. Carrying out parametric analyses of nonlinear systems can be computationally expensive because of the required computation of the forced response curves (FRC) for all considered points of the design space. Bifurcation tracking is particularly attractive as it consists in only following the evo-

*Corresponding author
adrien.melot@ec-lyon.fr (A. Mélot)
ORCID(s):

lution of bifurcation points, reducing the number of computed points to the number of bifurcations. Another benefit of directly following bifurcation points is that a folding of the bifurcation curves can reveal isolated responses, i.e., responses that are not connected to the main solution branch [1, 15].

The objectives of this work are twofold: to introduce bifurcation tracking as a efficient tool to design tooth profile modifications in order to mitigate the nonlinear dynamic response of the system and to investigate the influence of uncertainty on the optimal tooth profile modifications. The present paper is structured as follows: the mathematical model of the gear pair is introduced in Sect. 2. The computational strategy and uncertainty modelling is detailed in Sect. 3. Results are discussed in Sect. 4 and main conclusions are drawn in Sect. 5.

2. Mathematical model of the gear pair

2.1. Equation of motion of the gear pair

The geared system used in this paper is a spur gear pair whose gear ratio is equal to 1. The gears are modelled as two rigid disks with respective inertia I_1 and I_2 and rotational degrees of freedom (DoF) θ_1 and θ_2. A nonlinear elastic force, noted f_{nl}, representing the contact between gear teeth acts along the line of action, i.e. in the normal direction of the tooth profile.

The equations of motion of this two-degree-of-freedom model are:

$$\begin{cases} I_1\ddot{\theta}_1 - T_1 + r_{b,1} f_{nl} = 0 \\ I_2\ddot{\theta}_2 + T_2 - r_{b,2} f_{nl} = 0 \end{cases} \tag{1}$$

where $T_1 = T_2 = 100$ N·m are respectively the input and output torques and $r_{b,k}$ denotes the base radius of gear k. The transmission error $q = r_{b,1}\theta_1 - r_{b,2}\theta_2$ can be introduced at this stage in order to remove the rigid body motion corresponding to the rotation of the gear pair. The resulting equation of motion reads:

$$M_{eq}\ddot{q} + f_{nl}(q,t) = F_s \tag{2}$$

with the equilavent mass M_{eq} and static mesh force F_s:

$$\begin{cases} M_{eq} = \frac{I_1 I_2}{r_{b,1}^2 I_2 + r_{b,2}^2 I_1} \\ F_s = \frac{T_1}{r_{b,1}} = \frac{T_2}{r_{b,2}} \end{cases} \tag{3}$$

2.2. Gear coupling

The nonlinear mesh force f_{nl} describes an elastic coupling when the gears are in contact and must be able to model potential contact loss and resulting impacts between gear teeth.

2.2.1. Backlash nonlinearity

Linerarizing the transmitted load around the static equilibrium, i.e. the static transmission error q_s, allows one to define, for each angular position θ_1, a mesh stiffness $k_m(\theta_1)$ coupling the two gears in contact:

$$k_m(\theta_1) = \frac{\partial F_s}{\partial q_s(\theta_1)} \tag{4}$$

Note that for non-zero rotational speeds $k_m(\theta_1) = k_m(\Omega t)$. Due to the linearization, the contact force associated to the mesh stiffness equals zero for a positive displacement if:

$$q(t) \leq g(t) = b + q_s(t) - \frac{F_s}{k_m(t)} \tag{5}$$

where b is half backlash, considered constant in the following. The mesh force (cf. Fig. 2) including the backlash nonlinearity can therefore be expressed as:

$$\begin{aligned} f_{nl}(q,t) &= k_m(t)\,(q - g(t))\,\mathcal{H}(q - g(t)) \\ &+ k_m(t)\,(q + g(t))\,\mathcal{H}(-q - g(t)) \end{aligned} \tag{6}$$

where $\mathcal{H}$ is the Heaviside step function.

2.2.2. Damping

In the following, we consider an equivalent viscous damping that does not depend on the contact state [21, 11, 28, 29].

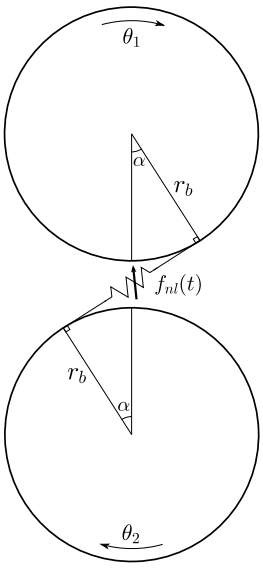

Figure 1: Nonlinear gear model.

Table 1
Characteristics of the gear pair

Name		Gear 1	Gear 2	Unit
Module	m	2		mm
Number of teeth	Z	50	50	-
Pressure angle	α	20		deg
Base radius	r_b	46.984	46.984	mm
Profile shift coefficient	x	0	0	-
Addendum coefficient	h_a	1	1	-
Dedendum coefficient	h_d	1.25	1.25	-
Face width	b_f	20		mm
Inertia	I_1	1.52e-3	1.52e-3	kg.m^2

The damping term reads:

$$C = 2\xi\sqrt{\bar{k}_m M_{eq}} \tag{7}$$

where $\bar{k}_m$ is the mean value of the periodic mesh stiffness and ξ the damping ratio. Thus, the complete equation of motion of the gear pair is:

$$M_{eq}\ddot{q} + C\dot{q} + f_{nl}(q,t) = F_s \tag{8}$$

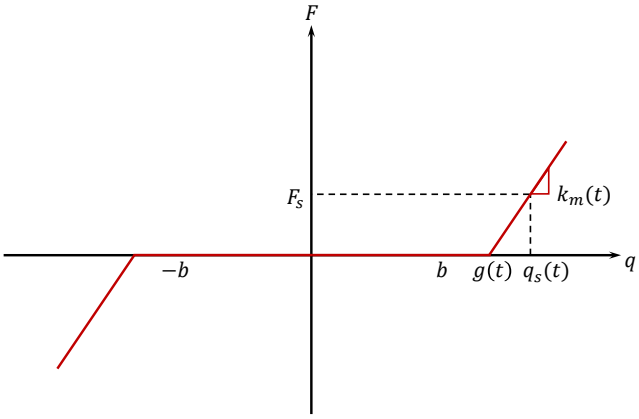

Figure 2: Nonlinear force model for a given angular position of the gear pair.

3. Computational strategy and uncertainty modelling

Monte-Carlo simulations [26] are commonly used in dynamic analyses in order to propagate uncertainties. Despite their widespread use, such simulations often lead to hefty computational effort due to the large number of samples and computations of the forced response curves required to ensure convergence. To avoid such issues, the proposed approach is based on a deterministic computation of the bifurcation curves of the investigated system. This reduces the number of points to compute for each value of the uncertain parameter to the number of identified bifurcations. Herein, bifurcation tracking analysis is applied to the amount of tip relief, corresponding to an intentional removal of material at the tip of the gear teeth (see. Fig. 3). The study focuses on minimizing the dynamic response around the primary resonance, especially the amplitude-jump phenomenon induced by the folding of the response curve delimited by two saddle-node (SN) bifurcations. The location of bifurcation points with respect to this parameter are obtained with minimal computational effort using the methodology thoroughly detailed in [29]. For the sake of completeness a short description is provided hereafter.

3.1. Nonlinear solver

The periodic solutions of equation (8) are sought as truncated Fourier series:

$$q \approx \mathrm{Re}\left(\sum_{k=0}^{H} \tilde{\mathbf{q}}_k e^{ik\Omega t}\right), \tag{9}$$

Eq. (9) and its time derivatives are plugged into the equation of motion (8) and Galerkin projection is performed with the same harmonic base functions to obtain a system of nonlinear algebraic equations. An arc-length continuation procedure [35] with a tangent predictor is then used to follow the evolution of the solution point with respect to the forcing (rotational) frequency Ω. At each iteration, the nonlinear mesh force is evaluated from Eq. (6) with the alternating frequency/time (AFT) algorithm [4].

In order to track bifurcation points with respect to an additional parameter, a minimaly extended system is built by appending an additional equation to the system [13, 7, 29]. The bifurcation equation, noted G, is evaluated through the resolution of a linear system of equations which depends on the bifurcation being tracked:

$$\begin{bmatrix} \mathbf{A} & \mathbf{b} \\ \mathbf{d}^\dagger & 0 \end{bmatrix} \begin{pmatrix} \mathbf{w} \\ G \end{pmatrix} = \begin{pmatrix} \mathbf{0} \\ 1 \end{pmatrix} \tag{10}$$

where vectors $\mathbf{b}$ and $\mathbf{d}$ are bordering vector that ought to ensure that system (10) is nonsingular and superscript $\dagger$ denotes the Hermitian transpose. Matrix A is the Jacobian matrix of the system with respect to the unknown Fourier coefficients when saddle-node (SN) bifurcations are tracked. For computational efficiency, the derivatives of the residual and arc-length equation are evaluated analytically. The derivatives of the bifurcation equation G are computed semi-analytically in parallel. The above described computational strategy relies on a Newton-Raphson solver which requires a initial guess sufficiently close to an actual solution point. For bifurcation tracking, a preliminary forced response curve is computed and bifurcation points are detected with a stability analysis based on Hill's method [27, 16, 23, 18, 31].

3.2. Static transmission error and mesh stiffness

During the computation of the bifurcations curves, the residual of the system and its derivatives have to be evaluated at values that are unknown beforehand. The computation of the nonlinear forces, given by Eq. (6), involves the STE and time-varying mesh stiffness (TVMS). Both heavily depend on the amount of tip relief μ and are periodic under stationary operating conditions. The strategy employed hereafter [29] consists in expressing the STE, TVMS and their derivatives with respect to the amount of tip relief μ as truncated Fourier series with interpolated Fourier coefficients:

$$\begin{cases} q_s(\mu,t) = \sum_{k=0}^{H_{q_s}} q_s^{c,k}(\mu)\cos(k\Omega t) + q_s^{s,k}(\mu)\sin(k\Omega t) \\ k_m(\mu,t) = \sum_{k=0}^{H_{k_m}} k_m^{c,k}(\mu)\cos(k\Omega t) + k_m^{s,k}(\mu)\sin(k\Omega t) \\ \partial_\mu q_s(\mu,t) = \sum_{k=0}^{H_{q_s}} \partial_\mu q_s^{c,k}(\mu)\cos(k\Omega t) + \partial_\mu q_s^{s,k}(\mu)\sin(k\Omega t) \\ \partial_\mu k_m(\mu,t) = \sum_{k=0}^{H_{k_m}} \partial_\mu k_m^{c,k}(\mu)\cos(k\Omega t) + \partial_\mu k_m^{s,k}(\mu)\sin(k\Omega t) \end{cases} \tag{11}$$

where ∂_μ denotes the partial derivative with respect to the bifurcation tracking parameter, corresponding to the amount

of tip relief in the present study. The in-house solver TERRA (**T**ransmission **ERR**or **A**nalysis) [33, 12] is used to compute the STE and TVMS for several amounts of tip relief. Fast Fourier transforms (FFT) are performed and coefficients $q_s^{c,k}$, $q_s^{s,k}$, $k_m^{c,k}$ and $k_m^{s,k}$ are interpolated. The derivatives of the Fourier coefficients are then calculated analytically, directly within the AFT algorithm. For more details, the interested reader can refer to [29].

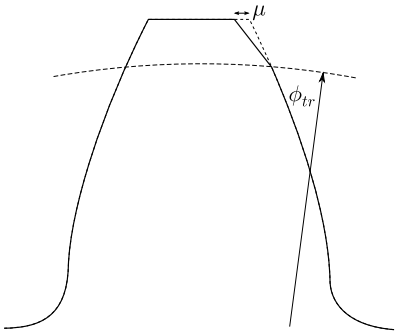

Figure 3: Schematic representation of a tip relief modification. μ is the amount of tip relief, ϕ_{tr} is starting radius of the profile modification ($\phi_{tr} = 50.26$ μm).

3.3. Uncertainty modelling

In present study, we consider an uncertain amount of tip relief μ on both gears. In order to evaluate its influence on the dynamic response of the system and resulting optimum TPM, we define two criteria. The nonlinearity can induce multiple co-existing solutions for a given set of parameters. As is well known, if the vibration amplitude is large enough, saddle-node bifurcations can appear and lead to potential amplitude-jumps under variations of the rotational speed or perturbations of the system.

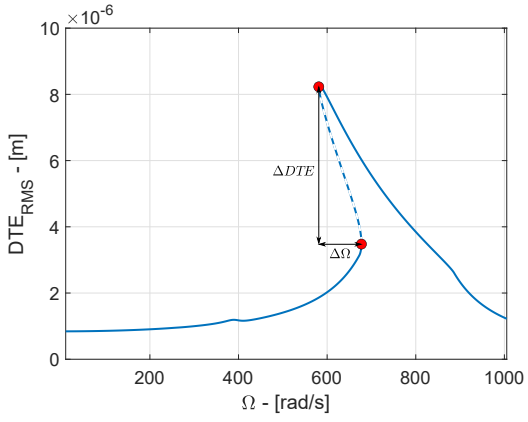

Figure 4: Example of forced response curve without tip relief modification ($\mu = 0$ μm). Solid and dashed lines denote stable and unstable responses, respectively. Saddle-node bifurcation points are represented by red circle markers.

In this work, we define the optimum TPM as the median amount of tip relief μ_{med} that best mitigates the severity of the amplitude jump phenomenon. We introduce two ad hoc criteria to be minimised, namely $\mathcal{C}_{freq}$ and $\mathcal{C}_{freq}$:

$$\mathcal{C}_{freq}(\mu) = \int_{\mu_{min}}^{\mu_{max}} \Delta\Omega(x) f_p(x) \mathrm{d}x \tag{12}$$

$$\mathcal{C}_{ampl}(\mu) = \int_{\mu_{min}}^{\mu_{max}} \Delta DTE(x) f_p(x) \mathrm{d}x \tag{13}$$

where $f_p(x)$ corresponds to a probability density function, $\Delta\Omega(x)$ and $\Delta DTE(x)$ are respectively the frequency and amplitude interval between the upper and lower SN bifurcation on the primary resonance (see Fig. 4). μ_{min} and μ_{max} are the bounds of the interval of variability. The size of the latter is herein taken equal to 5 μm with the lower bound $\mu_{min} \in [0, 10]$ μm. Negative values are not considered here, as it would imply added material.

Information regarding distribution laws of tooth profile modification is scarce, although a few sources report uniform, Gaussian or Weibull distributions. Due to the lack of information and in order to quantify the influence of the type of distribution on the results all three distributions as well as a beta distribution are considered in the following (see Fig. 5). The first two are symmetric while the Weibull and beta distributions are asymmetric in most cases, depending on the chosen parameters.

The uniform distribution depends on the lower and upper bounds of the uncertainty interval such that:

$$f_p(x) = \frac{1}{\mu_{max} - \mu_{min}}, \quad \forall x \in [\mu_{min}, \mu_{max}] \tag{14}$$

The normal distribution is expressed with its mean value $\mu = (\mu_{min} + \mu_{max})/2$ and its standard deviation σ such that $3\sigma = (\mu_{min} - \mu_{max})/2$:

$$f_p(x) = \frac{1}{\sigma\sqrt{2\pi}} \exp\left(-\frac{1}{2}\left(\frac{x-\mu}{\sigma}\right)^2\right) \tag{15}$$

The Weibull distribution has the following expression:

$$f_p(x) = \frac{k}{\lambda}\left(\frac{x-\theta}{\lambda}\right)^{k-1} \exp\left(-\left(\frac{x-\theta}{k}\right)^k\right), \forall x \geq \theta \tag{16}$$

where k and λ are the shape and scale parameters. Parameter θ is a location parameter allowing for an offset of the distribution on the x-axis to account for the varying lower bound of the interval of uncertainty. The shape and scale parameters chosen in this study are $k = 1.75$ and $\lambda = 2$, respectively, which results in a "left-skewed" distribution.

The beta distribution considered hereafter is expressed:

$$f_{beta}(x) = \frac{\Gamma(\alpha+\beta)}{\Gamma(\alpha)\Gamma(\beta)} x^{\alpha-1}(1-x)^{\beta-1}, \quad \forall x \in [0, 1] \tag{17}$$

where Γ is the gamma function and α and β are shape parameters whose value are $\alpha = 2.5$ and $\beta = 2$ in this study, resulting in a "right-skewed" distribution. The beta distribution is defined for $x \in [0, 1]$. In the following, the beta PDF is computed with $x \in [\mu_{min}, \mu_{max}]$ and normalized, i.e.:

$$f_p(x) = \frac{f_{beta}\left(\frac{x-\mu_{min}}{\mu_{max}-\mu_{min}}\right)}{\mu_{max} - \mu_{min}} \tag{18}$$

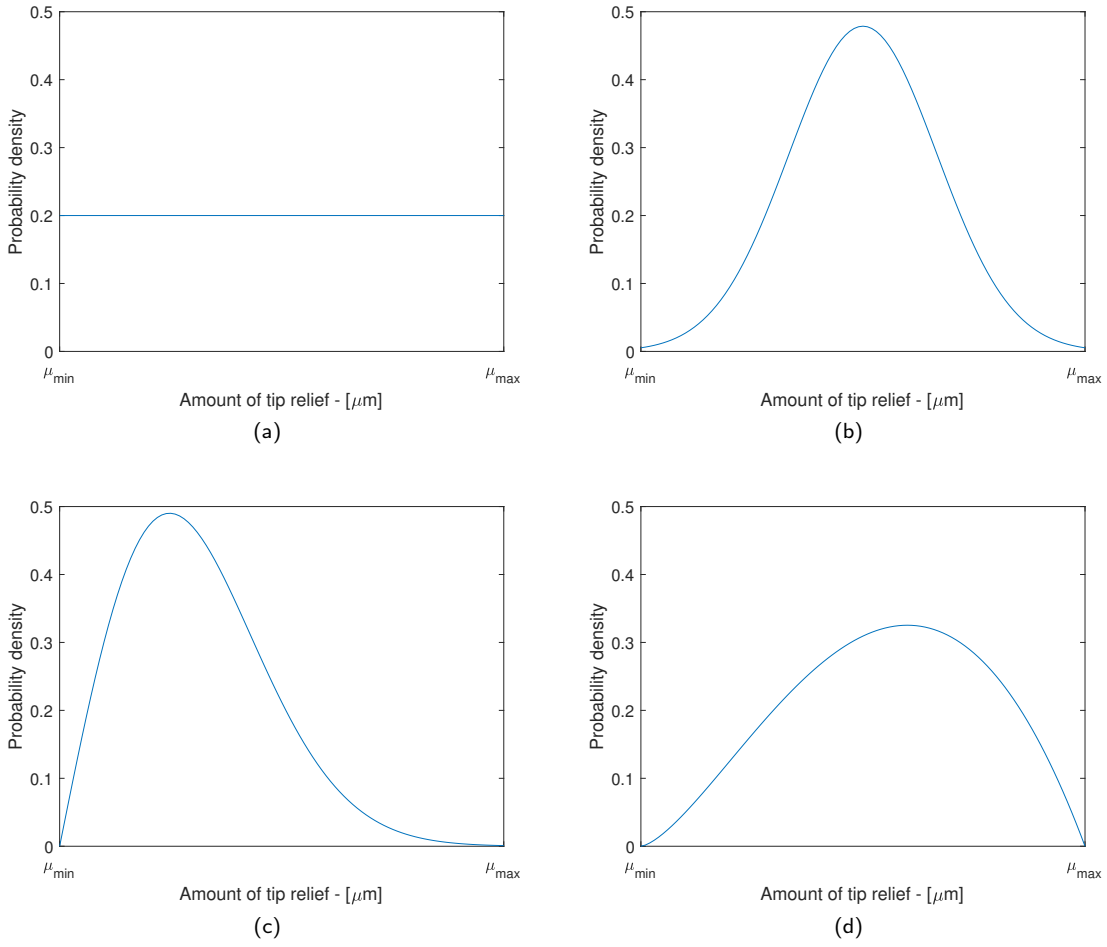

Figure 5: Probability density functions considered for the uncertain tip relief parameter. (a) Uniform distribution (b) Normal distribution, (c) Weibull distribution with parameters $\lambda = 1.75$ and $k = 2$, (d) beta distribution with parameters $\alpha = 2.5$ and $\beta = 2$.

4. Results and discussion

4.1. Optimization of the static transmission error with respect to the amount of tip relief

In order to highlight the benefits of the proposed methodology, we first discuss the choice of tip relief to minimize the excitation induced by the meshing process, as is standard practice in gear design. The static transmission error is computed for each value of the amount of tip relief in the discretized design interval $\mathcal{T} = [0\ 15]$ μm.

Figure 6 shows the evolution of the peak-to-peak STE with respect to the amount of tip relief for the input torque $T = 100$ N·m. The STE_{PP} first decreases as the amount of tip relief is increased. The peak-to-peak value decreases from 2.1 μm with no tip relief to 1.2 μm when the amount of tip relief reaches 3 μm, which will be henceforth referred to as static optimum. The STE_{PP} then increases with the amount of tip relief.

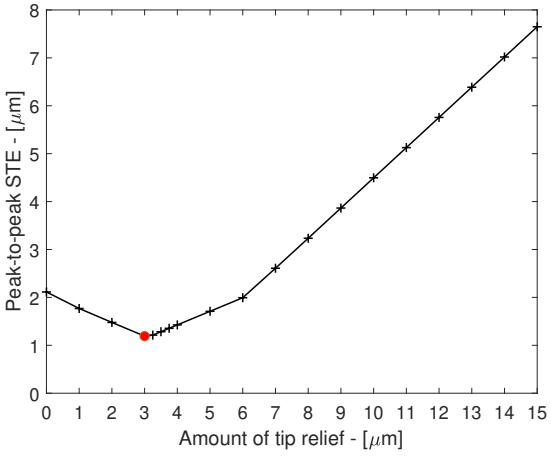

Figure 6: Evolution of the peak-to-peak static transmission error with respect to the amount of tip relief. The red dot denotes the optimum solution, corresponding to the smallest peak-to-peak value of the static transmission error

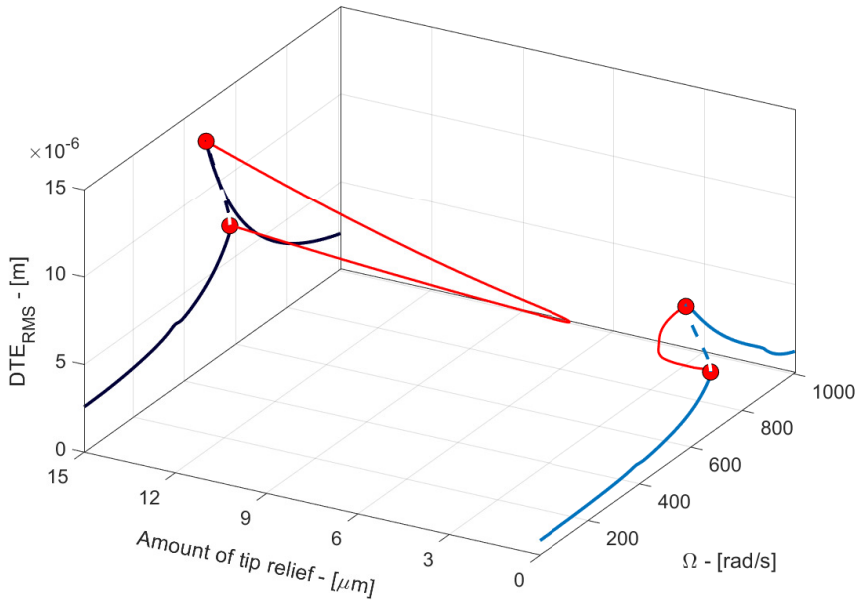

(a) 3D space

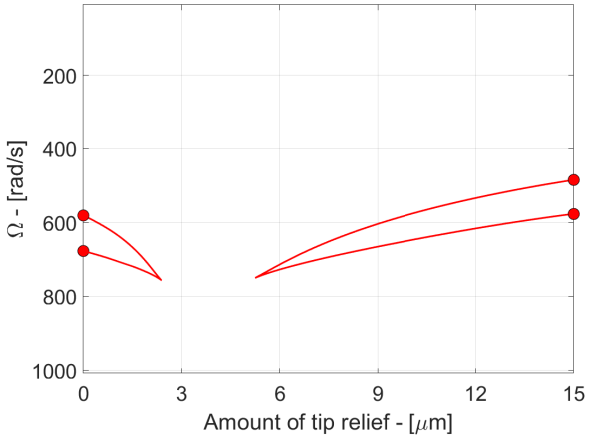

(b) Frequency-tip relief plane

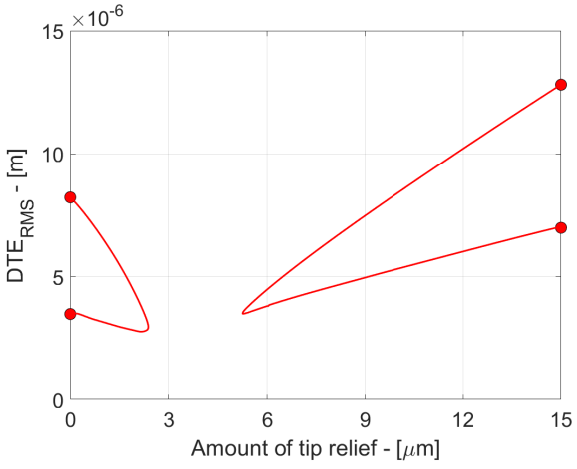

(c) Amplitude-tip relief plane

Figure 7: Saddle-node bifurcation curves. The blue lines represent the forced response curves; saddle-node bifurcation points are represented by red circle markers and red lines denote the bifurcation curves.

4.2. Optimization of the dynamic behaviour with respect to the uncertain amount of tip relief

The first step of the proposed methodology is to compute the bifurcation curves with respect to the uncertain parameter. The number of sampling points used in the AFT algorithm is $N_s = 2^{11}$ and the list of harmonics for the HBM is $H = (0, 50, 100, 150, 200, 250, 300, 350)$, corresponding to harmonics of the meshing frequency H_{50}. The bifurcation tracking algorithm requires an initial guess close to the location of a bifurcation point in the design space. Two preliminary forced response analyses are carried out at each end of the interval of variability, i.e. for $\mu = 0$ μm and $\mu = 15$ μm. A stability analysis allows one to detect two SN bifurcations on each curve. The SN bifurcations located at the top of the primary resonances are chosen as initial guesses.

Figure 7 shows the SN bifurcation curves computed with the tracking algorithm with respect to the excitation (rotational) frequency and amount of tip relief. The root mean square value of the fluctuations of dynamic transmission error, DTE_{RMS}, is chosen as a measure of the response amplitude. Figures 7b and 7c show the bifurcation curves in the frequency-tip relief and amplitude-tip relief planes, respectively. The tracking reveals two unstable zones delimited by the saddle-node bifurcations, i.e. the red lines, where multiple solution coexist and a small zone that doesn't exhibit amplitude-jump instability in between.

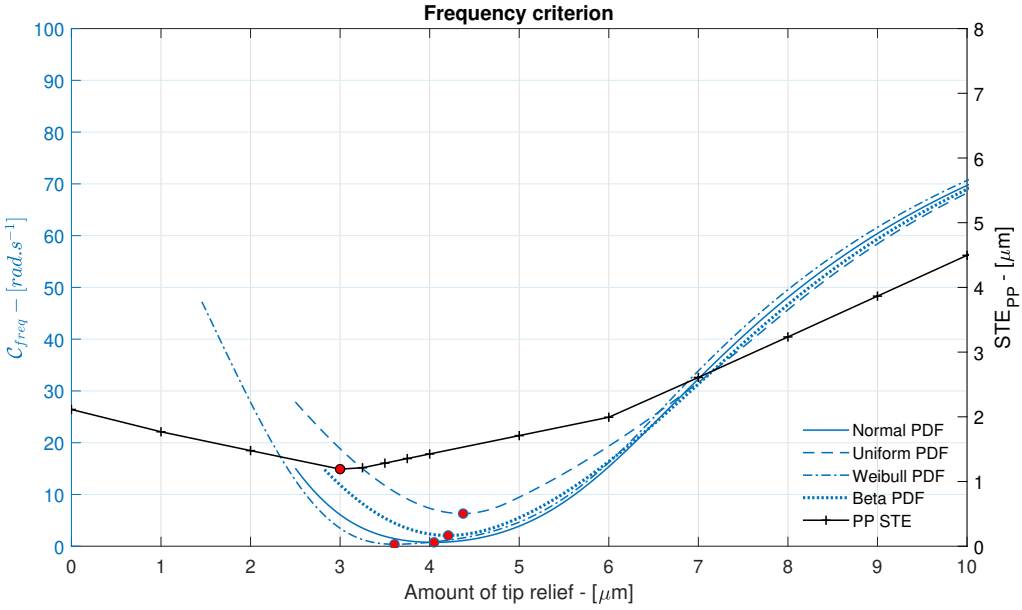

(a)

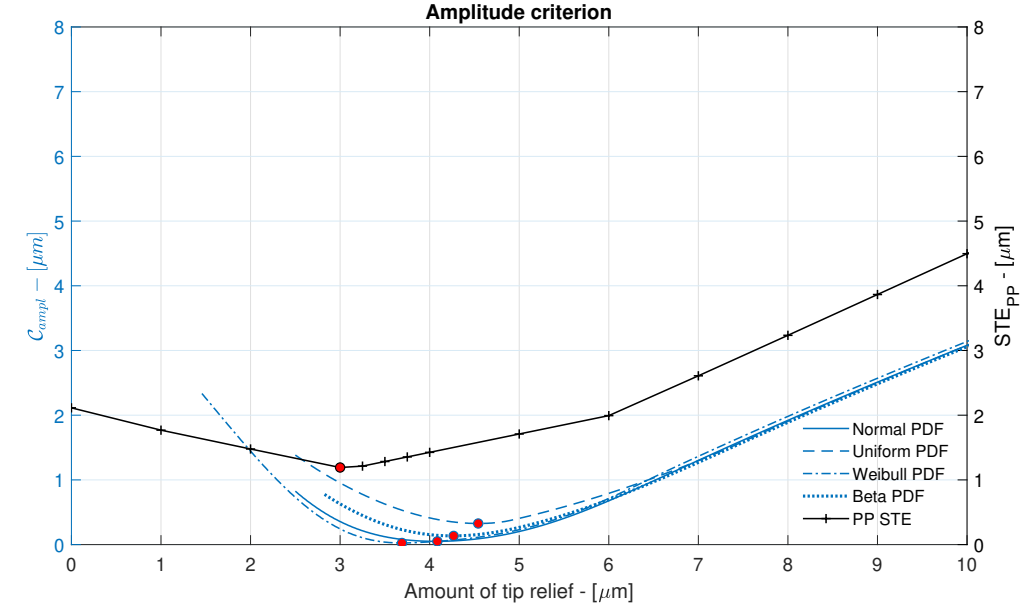

(b)

Figure 8: Evolution of the frequency criterion (a) and amplitude criterion (b) with respect to the amount of tip relief. Red circle markers denote the optimal value of tip relief. The evolution of the peak-to-peak STE is represented as a black line with cross markers.

The first unstable zone exists for values of tip relief $\mu \in [0\ 2.4]$ μm, which is quite close to the optimal tip relief computed with static analyses. The second unstable zone appears for $\mu \geq 5.3$ μm. Interestingly, the shapes of the unstable zones in the frequency-tip relief plane (cf. Fig. 7b) are quite similar since the width $\Delta\Omega$ seems to stabilize at approximately $\Delta\Omega = 100$ rad/s. Nevertheless, the first unstable zone shows a rapid decline in the amplitude-tip relief plane (cf. Fig. 7c). Indeed, the width of the unstable zone is $\Delta DTE = 4.8$ μm at $\mu = 0$ μm and decreases rapidly until the two SN bifurcations coalesce and disappear at $\mu = 2.4$ μm. The width of the second unstable zone grows significantly slower as the tip relief increases. For instance, the SN bifurcations emerge at $\mu = 5.3$ μm and the width only reaches $\Delta DTE = 3.1$ μm at $\mu = 10$ μm.

To carry out the uncertainty analysis, the interval $\mathcal{V} = [0, 10]$ μm, in which the lower bound of the uncertainty interval varies, is discretized with 100 points. The uncertainty

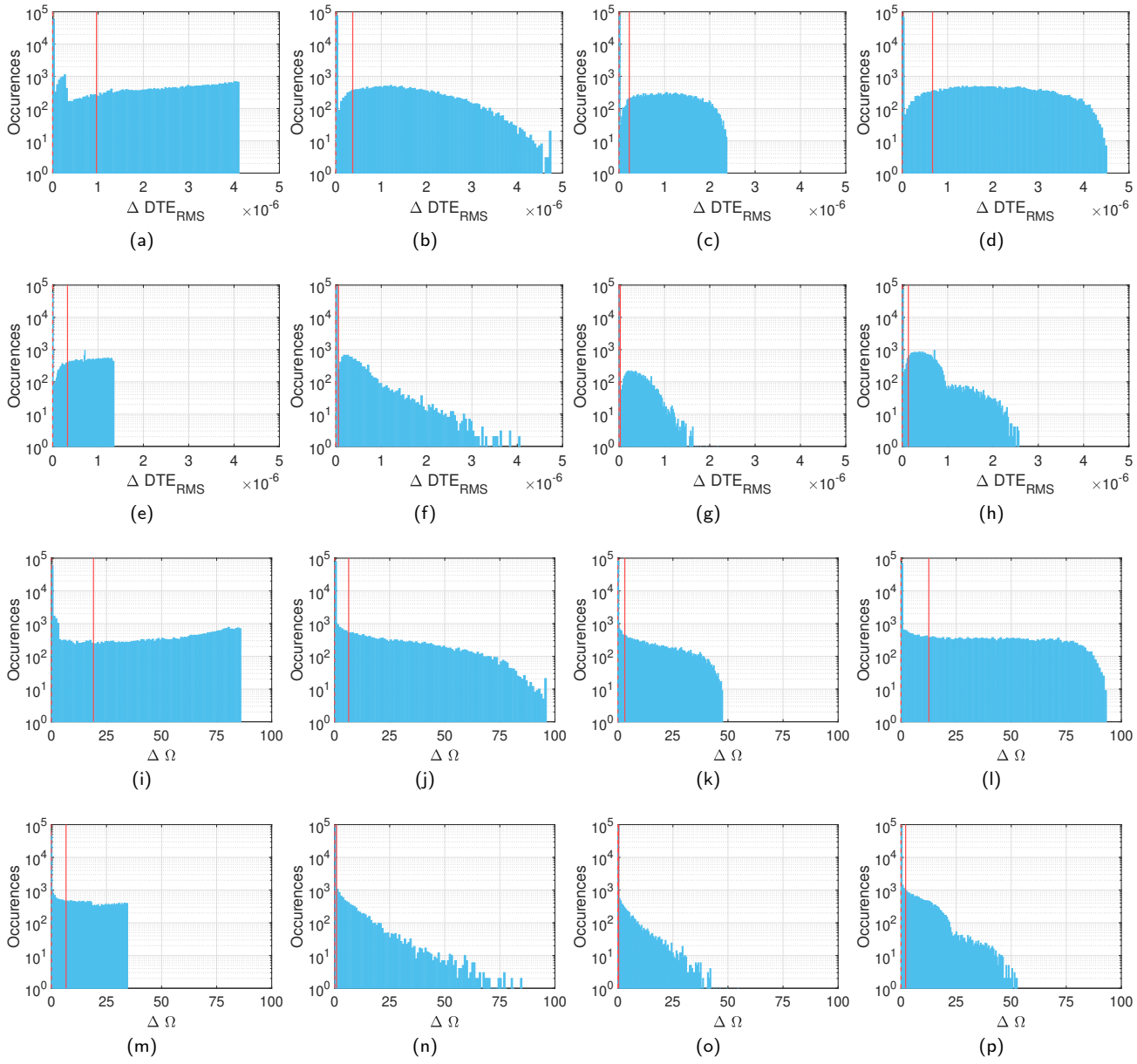

Figure 9: Probability density functions of the amplitude (a, b, c, d, e, f, g, h) and frequency intervals (i, j, k, l, m, n, o, p) between upper and lower SN bifurcations. PDF computed with MC simulations in the interval whose median equals the optimum obtained from static computations (a, b, c, d, i, j, k, l) and dynamic computations (e, f, g, h, m, n, o, p). (a, e, i, m) Uniform distribution, (b, f, j, n) Normal distribution, (c, g k, o) Weibull distribution with parameters $\lambda = 1.75$ and $k = 2$, (d, h, l, p) beta distribution with parameters $\alpha = 2.5$ and $\beta = 2$. The red solid lines denote the mean values while the red dashed lines represent the medians.

interval $\mu_{max} - \mu_{min}$ itself is discretized with an odd number of points, 101 in this study, for an accurate representation of the probability density functions. The criteria defined by Eq. (12) and (13) are computed for each value of the lower bound of the uncertainty interval with almost no additional computational effort using the results of the bifurcation tracking analysis. For each value of the lower bound μ_{min}, the median value of tip relief for each probability density function is stored.

Figure 8 shows the evolution of both criteria with respect to the median value of the amount of tip relief μ_{med}. Solid, dashed and dotted lines are associated to the criteria calculated with the different probability density functions. The peak-to-peak values of the STE are superimposed for easier comparison. The optimum amount of tip relief, i.e. the median tip relief associated to the smallest value of the criteria, for each considered probability density function is denoted with a red circle marker.

One can see that the optimal tip relief is shifted towards larger values compared with the STE computations. Interestingly, the type of probability density function used for the calculation has a moderate influence of the optimal value of tip relief, with all optimums located approximately at $\mu = 4\ \mu$m. Overall, both criteria have a similar evolution with the tip relief and yield somewhat similar results. One can also note that both criteria reach values close to zero at the optimal value of tip relief, indicating that amplitude-jump instabilities are well mitigated and almost non-existent.

This is confirmed by carrying out Monte-Carlo simulations from the bifurcation tracking results. For each distribution of the amount of tip relief, a Monte-Carlo simulation is performed within the uncertainty interval associated to the optimum amount of tip relief computed with the proposed methodology. Note that when the optimums obtained with the two criteria differ, the one minimizing C_{ampl} is used. Figure 9 shows the probability density functions of ΔDTE and $\Delta\Omega$ computed with $n_{MC} = 100000$ samples. For reference, MC simulations with the uncertainty interval associated to the static optimum, i.e. with a median equal to $\mu = 3\ \mu$m, is also carried out (cf. Fig. 9a-9d and Fig. 9i-9l). One can see that, for all cases, the probability density functions of both ΔDTE and $\Delta\Omega$ are utterly different from the probability density functions of the amount of tip relief. Besides, the majority of samples are characterized by an absence of amplitude jump as indicated by a median equal to zero. Furthermore, it appears that the dynamic optimum induces a shift of the mean value of both ΔDTE and $\Delta\Omega$ towards zero as well as a smaller standard deviation. Thus, amplitude-jump instabilities are better mitigated.

5. Conclusion

A computational procedure based on bifurcation tracking was proposed to design tooth profile modifications in the presence of uncertainties. The proposed approach allows one to analyze the influence of uncertainty in tooth profile modifications on the nonlinear dynamic response of a gear pair and to define a optimal design. It was found that considering uncertainties leads to a different optimal value of the tooth profile modification compared to the one obtained with static computations. Four probability density functions were considered in the analysis. Results suggest that their influence on the optimal value is limited.

The methodology was applied to the amount of tip relief but can be implemented with any type of tooth profile modification. At the moment, only one uncertain parameter can be investigated at a time. Future work may look into extending the methodology to higher co-dimensions. It can also be extended to large-scale geared system models using model order reduction techniques [25] without the need to resort to parametric reduced-order models [22] since the gear coupling is treated in physical coordinates. Finally, the approach can be extended to other types of bifurcation (Neimark-Sacker, period-doubling) for better designs.

Acknowledgements

This work was performed within the LabCom LADAGE (LAboratoire de Dynamique des engrenAGEs), created by the LTDS and the Vibratec Company and operated by the French National Research Agency (ANR-14-LAB6-0003). It was also performed within the framework of the LABEX CeLyA (ANR-10-LABX-0060) of Université de Lyon, within the program "Investissements d'Avenir" (ANR-16-IDEX-0005) operated by the French National Research Agency (ANR).

Conflict of interest

The authors declare that they have no conflict of interest.

CRediT authorship contribution statement

Adrien Mélot: Conceptualization, Methodology, Software, Validation, Investigation, Data Curation, Writing - Original Draft, Writing - Review and Editing. **Emmanuel Rigaud:** Conceptualization, Funding acquisition, Writing - Review and Editing. **Joël Perret-Liaudet:** Conceptualization, Funding acquisition, Writing - Review and Editing.

References

[1] Alcorta, R., Baguet, S., Prabel, B., Piteau, P., Jacquet-Richardet, G., 2019. Period doubling bifurcation analysis and isolated subharmonic resonances in an oscillator with asymmetric clearances. Nonlinear Dynamics 98, 2939–2960. doi:https://doi.org/10.1007/s11071-019-05245-6.

[2] Beyaoui, M., Tounsi, M., Abboudi, K., Feki, N., Walha, L., Haddar, M., 2016. Dynamic behaviour of a wind turbine gear system with uncertainties. Comptes Rendus Mécanique 344, 375–387. URL: https://www.sciencedirect.com/science/article/pii/S1631072116000048, doi:https://doi.org/10.1016/j.crme.2016.01.003.

[3] Bonori, G., Barbieri, M., Pellicano, F., 2008. Optimum profile modifications of spur gears by means of genetic algorithms. Journal of Sound and Vibration 313, 603–616. doi:https://doi.org/10.1016/j.jsv.2007.12.013.

[4] Cameron, T.M., Griffin, J., 1989. An Alternating Frequency/Time Domain Method for Calculating the Steady-State Response of Nonlinear Dynamic Systems. Journal of Applied Mechanics. doi:https://doi.org/10.1115/1.3176036.

[5] Carbonelli, A., Perret-Liaudet, J., Rigaud, E., Le Bot, A., 2011. Particle Swarm Optimization as an Efficient Computational Method in order to Minimize Vibrations of Multimesh Gears Transmission. Advances in Acoustics and Vibration 2011, 195642. doi:https://doi.org/10.1155/2011/195642. publisher: Hindawi Publishing Corporation.

[6] Carbonelli, A., Rigaud, E., Perret-Liaudet, J., 2016. Vibro-Acoustic Analysis of Geared Systems—Predicting and Controlling the Whining Noise. Springer International Publishing, Cham. pp. 63–79. doi:10.1007/978-3-319-24055-8_5.

[7] Detroux, T., Renson, L., Masset, L., Kerschen, G., 2015. The harmonic balance method for bifurcation analysis of large-scale nonlinear mechanical systems. Computer Methods in Applied Mechanics and Engineering 296, 18–38. doi:https://doi.org/10.1016/j.cma.2015.07.017.

[8] Driot, N., Perret-Liaudet, J., 2006. Variability of modal behavior in terms of critical speeds of a gear pair due to manufacturing errors and shaft misalignments. Journal of Sound and Vibration 292, 824–843. URL: https://www.sciencedirect.com/science/article/pii/S0022460X05006747, doi:https://doi.org/10.1016/j.jsv.2005.09.031.

[9] Driot, N., Rigaud, E., Sabot, J., Perret-Liaudet, J., 2001. Allocation of gear tolerances to minimize gearbox noise variability. Acta Acustica united with Acustica 87, 67–76. doi:https://doi.org/10.1016/j.jsv.2014.02.008.

[10] Faggioni, M., Samani, F.S., Bertacchi, G., Pellicano, F., 2011. Dynamic optimization of spur gears. Mechanism and Machine Theory 46, 544–557. URL: https://www.sciencedirect.com/science/article/pii/S0094114X10002028, doi:https://doi.org/10.1016/j.mechmachtheory.2010.11.005.

[11] Farshidianfar, A., Saghafi, A., 2014. Global bifurcation and chaos analysis in nonlinear vibration of spur gear systems. Nonlinear Dynamics 75, 783–806. doi:https://doi.org/10.1007/s11071-013-1104-4.

[12] Garambois, P., Perret-Liaudet, J., Rigaud, E., 2017. NVH robust optimization of gear macro and microgeometries using an efficient tooth contact model. Mechanism and Machine Theory 117, 78 – 95. doi:https://doi.org/10.1016/j.mechmachtheory.2017.07.008.

[13] Govaerts, W., Kuznetsov, Y., Dhooge, A., 2005. Numerical continuation of bifurcations of limit cycles in matlab. SIAM Journal ON Scientific Computing 27, 231–252.

[14] Gregory, R.W., Harris, S.L., R. G. Munro, G., 1963. Dynamic behaviour of spur gears. Proceedings of the Institution of Mechanical Engineers 178, 207–218. doi:10.1177/002034836317800130.

[15] Grenat, C., Baguet, S., Lamarque, C.H., Dufour, R., 2019. A multi-parametric recursive continuation method for nonlinear dynamical systems. Mechanical Systems and Signal Processing 127, 276–289. doi:https://doi.org/10.1016/j.ymssp.2019.03.011.

[16] Groll, G.V., Ewins, D., 2001. The harmonic balance method with arc-length continuation in rotor/stator contact problems. Journal of Sound and Vibration 241, 223 – 233. doi:https://doi.org/10.1006/jsvi.2000.3298.

[17] Guerine, A., El Hami, A., Walha, L., Fakhfakh, T., Haddar, M., 2015. A perturbation approach for the dynamic analysis of one stage gear system with uncertain nnparameters. Mechanism and Machine Theory 92, 113–126. URL: https://www.sciencedirect.com/science/article/pii/S0094114X15001093, doi:https://doi.org/10.1016/j.mechmachtheory.2015.05.005.

[18] Guillot, L., Lazarus, A., Thomas, O., Vergez, C., Cochelin, B., 2020. A purely frequency based floquet-hill formulation for the efficient stability computation of periodic solutions of ordinary differential systems. Journal of Computational Physics 416, 109477. doi:https://doi.org/10.1016/j.jcp.2020.109477.

[19] Hotait, M., Kahraman, A., 2013. Experiments on the relationship between the dynamic transmission error and the dynamic stress factor of spur gear pairs. Mechanism and Machine Theory 70, 116–128. URL: https://www.sciencedirect.com/science/article/pii/S0094114X13001389, doi:https://doi.org/10.1016/j.mechmachtheory.2013.07.006.

[20] Kahraman, A., Blankenship, G.W., 1999. Effect of Involute Tip Relief on Dynamic Response of Spur Gear Pairs. Journal of Mechanical Design 121, 313–315. doi:https://doi.org/10.1115/1.2829460.

[21] Kahraman, A., Singh, R., 1990. Non-linear dynamics of a spur gear pair. Journal of Sound and Vibration 142, 49–75. doi:10.1016/0022-460X(90)90582-K.

[22] Krack, M., Tatzko, S., Panning-von Scheidt, L., Wallaschek, J., 2014. Reliability optimization of friction-damped systems using nonlinear modes. Journal of Sound and Vibration 333, 2699–2712. URL: https://www.sciencedirect.com/science/article/pii/S0022460X14001138, doi:https://doi.org/10.1016/j.jsv.2014.02.008.

[23] Lazarus, A., Thomas, O., 2010. A harmonic-based method for computing the stability of periodic solutions of dynamical systems. Comptes Rendus Mécanique 338, 510 – 517. doi:https://doi.org/10.1016/j.crme.2010.07.020.

[24] Liu, G., Parker, R.G., 2008. Dynamic Modeling and Analysis of Tooth Profile Modification for Multimesh Gear Vibration. Journal of Mechanical Design 130. URL: https://doi.org/10.1115/1.2976803, doi:10.1115/1.2976803. _eprint: https://asmedigitalcollection.asme.org/mechanicaldesign/article-pdf/130/12/121402/6730960/121402_1.pdf.

[25] Mélot, A., Perret-Liaudet, J., Rigaud, E., 2022. Vibro-impact dynamics of large-scale geared systems. Preprint.

[26] Metropolis, N., Ulam, S., 1949. The monte carlo method. Journal of the American Statistical Association 44, 335–341. doi:10.1080/01621459.1949.10483310.

[27] Moore, G., 2005. Floquet theory as a computational tool. SIAM Journal on Numerical Analysis 42, 2522–2568.

[28] Mélot, A., Benaïcha, Y., Rigaud, E., Perret-Liaudet, J., Thouverez, F., 2022a. Effect of gear topology discontinuities on the nonlinear dynamic response of a multi-degree-of-freedom gear train. Journal of Sound and Vibration 516, 116495. doi:https://doi.org/10.1016/j.jsv.2021.116495.

[29] Mélot, A., Rigaud, E., Perret-Liaudet, J., 2022b. Bifurcation tracking of geared systems with parameter-dependent internal excitation. Nonlinear Dynamics 107, 413–431. doi:https://doi.org/10.1007/s11071-021-07018-6.

[30] Ozturk, V., Cigeroglu, E., Özgüven, H., 2014. Optimum profile modifications for the minimization of dynamic transmission error, in: International Gear Conference 2014: 26th–28th August 2014, Lyon. Oxford, pp. 596–605. doi:https://doi.org/10.1533/9781782421955.596.

[31] Peletan, L., Baguet, S., Torkhani, M., Jacquet-Richardet, G., 2013. A comparison of stability computational methods for periodic solution of nonlinear problems with application to rotordynamics. Nonlinear Dynamics 72, 671–682. doi:https://doi.org/10.1007/s11071-012-0744-0.

[32] Pfeiffer, F., Prestl, W., 1994. Hammering in diesel-engine driveline systems. Nonlinear Dynamics 5, 477–492. doi:10.1007/BF00052455.

[33] Rigaud, E., Barday, D., 1999. Modelling and Analysis of Static Transmission Error. Effect of Wheel Body Deformation and Interactions between Adjacent Loaded Teeth, in: 4th World Congress on Gearing and Power Transmission,, Paris, France. pp. 1961–1972.

[34] Rigaud, E., Perret-Liaudet, J., 2020. Investigation of gear rattle noise including visualization of vibro-impact regimes. Journal of Sound and Vibration 467, 115026. doi:https://doi.org/10.1016/j.jsv.2019.115026.

[35] Seydel, R., 2010. Practical Bifurcation and Stability Analysis. Springer-Verlag New York. doi:https://doi.org/10.1007/978-1-4419-1740-9.

[36] Tavakoli, M.S., Houser, D.R., 1986. Optimum Profile Modifications for the Minimization of Static Transmission Errors of Spur Gears. Journal of Mechanisms, Transmissions, and Automation in Design 108, 86–94. URL: https://doi.org/10.1115/1.3260791, doi:10.1115/1.3260791. _eprint: https://asmedigitalcollection.asme.org/mechanicaldesign/article-pdf/108/1/86/5481945/86_1.pdf.

[37] Tobe, T., Sato, K., 1977. Statistical analysis of dynamic loads on spur gear teeth. Bulletin of JSME 20, 882–889. doi:10.1299/jsme1958.20.882.

[38] Tobe, T., Sato, K., Takatsu, N., 1977. Statistical analysis of dynamic loads on spur gear teeth : Experimental study. Bulletin of JSME 20, 1315–1320. doi:10.1299/jsme1958.20.1315.

[39] Wei, S., Han, Q.K., Dong, X.J., Peng, Z.K., Chu, F.L., 2017. Dynamic response of a single-mesh gear system with periodic mesh stiffness and backlash nonlinearity under uncertainty. Nonlinear Dynamics 89, 49–60. URL: https://doi.org/10.1007/s11071-017-3435-z, doi:10.1007/s11071-017-3435-z.

[40] Welbourn, D., 1979. Fundamental knowledge of gear noise: A survey, in: Proceedings of conf. on Noise and Vibrations of Engines and Transmissions. C177/79, pp. 9-29.

[41] Xie, L., Baguet, S., Prabel, B., Dufour, R., 2017. Bifurcation tracking by harmonic balance method for performance tuning of nonlinear dynamical systems. Mechanical Systems and Signal Processing 88, 445–461. doi:https://doi.org/10.1016/j.ymssp.2016.09.037.